PERGAMON

Journal of Structural Geology 24 (2002) 107–122

JOURNAL OF STRUCTURAL GEOLOGY

www.elsevier.com/locate/jstrugeo

Evolution of fracture networks in shear zones: Insights from see-through experiments on biphenyl aggregates

Jürgen E. Streit[1,*], Stephen F. Cox[2]

Department of Geology, The Australian National University, Canberra, ACT 0200, Australia

Received 20 December 1999; revised 27 March 2001; accepted 29 March 2001

Abstract

Evolution of fracture porosity in mid-crustal shear zones can be simulated in in-situ experiments. Evolution of fracture networks was monitored during simple shearing of 2-mm-wide zones in wet and dry aggregates of polycrystalline biphenyl ($C_6H_5C_6H_5$) in a Urai–Means see-through deformation apparatus. At low effective confining pressures in wet samples, mixed brittle-viscous deformation occurred at all strain rates (5.6×10^{-4}–$5.8 \times 10^{-6}\ s^{-1}$) at 94–97% of the absolute melting temperature. At the fastest strain rate, progressive shearing is rapidly localized to produce a narrow fault zone along a shear zone boundary. In contrast, at the slowest strain rate, fractures develop throughout the shear zone and connect to form continuous fracture systems at low shear strains ($\gamma \approx 2$). These fracture systems accommodate most of the subsequent displacement in contrast to little fracturing and predominantly viscous deformation in a nominally dry experiment. Jogs, as parts of stairstepping fracture networks in wet samples, resemble in shape and distribution veins found in mid- to lower crustal shear zones. The experiments indicate that, from low strains onwards, the presence of fluids close to confining pressure in creeping shear zones can lead to the development of connected fracture networks that also localize most of the displacement.

Keywords: Fracture networks; Shear zones; Biphenyl aggregates; See-through experiments

1. Introduction

Shear veins and fault jogs filled with mineral precipitates are found in shear zones exhumed from shallow crustal depths (e.g. de Roo and Weber, 1992; Stel and Lankreyer, 1994) to mid and deep crustal levels (e.g. Boullier and Robert, 1992; Henderson and McCaig, 1996; Nguyen et al., 1998). Such veins are recognized as remnants of ancient fluid flow systems in the Earth's crust that have facilitated transport of hydrothermal fluids (e.g. Kerrich, 1986; Cox et al., 1987; Robert et al., 1995), and melts (Handy and Streit, 1999). However, we know little about the evolution of fracture porosity and its connectivity in active shear zones, as fracture systems are usually strongly deformed during continued deformation (e.g. de Roo and Weber, 1992; Law, 1998; Simpson, 1998; Streit and Cox 1998). Thus, it is not always clear in which orientation veins form in shear zones, and how they are interconnected to facilitate fluid transport. In addition, fluid pathways are not necessarily preserved by the development of mineral veins. For example, dissolution of quartz and other minerals that has led to substantial volume losses in some shear zones indicates large fluid fluxes (e.g. O'Hara, 1988; Glazner and Bartley, 1991; Selverstone et al., 1991), but fluid pathways are not indicated by the presence of veins. In this paper we argue that the development and evolution of connected fracture systems in mid to deep crustal shear zones can be simulated in see-through experiments on rock analog materials.

To investigate fluid transport properties of shear zones, the longevity of fractures also needs to be considered. For example, fluid infiltration may occur episodically in some mylonite zones via seismically generated fracture permeability (e.g. McCaig, 1988; McCaig et al., 1990). At crustal temperatures $\geqq 200°C$, seismically generated fracture permeability can be short lived on the time-scale of slip-recurrence ($\approx 10^2$–10^4 a) due to rapid fracture sealing in the presence of reactive fluids (e.g. Angevine et al., 1982; Brantley et al., 1990; Brantley, 1992). In contrast, permeability may persist during aseismic fault creep and permit continuous fluid flow especially at depths below the seismogenic regime (Cox, 1999). Effects that different

* Corresponding author. Fax: +61-(0)8-83034345.
E-mail address: jstreit@ncpgg.adelaide.edu.au (J.E. Streit).
[1] Now at National Centre for Petroleum Geology and Geophysics, The University of Adelaide, Thebarton Campus, SA 5005, Australia.
[2] Also at Research School of Earth Sciences, The Australian National University, Canberra, ACT 0200, Australia.

0191-8141/02/$ - see front matter
PII: S0191-8141(01)00052-9

shear rates and the presence of reactive pore fluids have on the evolution of fracture porosity and its connectivity during progressive shearing are investigated in in-situ shear experiments on biphenyl aggregates.

In this study we examine the evolution of fracture geometry and connectivity during high temperature shear deformation of biphenyl aggregates using a see-through shear apparatus. Experiments were conducted at high homologous temperatures (T_h) to allow for viscous deformation processes to occur at laboratory strain rates. We quantitatively examine the evolution of fracture geometry, length, and connectivity at different creep rates and in the presence of fluids in 2-mm-wide shear zones. Low experimental confining pressures, in combination with reactive fluids in the samples, are used to simulate low effective stress conditions at high pore fluid pressures in mid to lower crustal shear zones that have localized fluid flow. The experimental results have applications for understanding the geometry, style and scale of fracturing in natural shear zones. Furthermore, the observed evolution of fracture connectivity with increasing strain and at different strain rates provides insights about the evolution of fluid transport properties of active shear zones in the Earth's crust.

2. Sample preparation and experimental procedures

Deformation experiments on biphenyl ($C_6H_5C_6H_5$) were conducted in a Urai–Means see-through deformation apparatus (Urai, 1987; Means, 1989; Herwegh and Handy, 1996) in simple shear. Biphenyl, here used as a mineral analog, is monoclinic at room temperature (Charbonneau and Delugeard, 1977) and has a melting point at 70°C. Short prismatic grains transform at above ≈ 60°C to platy grains. The higher temperature phase is possibly orthorhombic (Bernstein et al., 1990).

To produce thin, polycrystalline samples of biphenyl, monoclinic biphenyl firstly was ground with a mortar and pestle. Because the material behaves predominantly brittle at room temperature, different techniques were tested and applied to produce thin sample discs. Three types of samples were prepared from powders. These are: (1) nominally dry and cold-pressed samples, (2) wet and cold-pressed samples, and (3) wet grain aggregates that were not cold pressed (slurry).

Wet samples were prepared by adding alcohol–water pore fluid mixtures (Table 1) to ground biphenyl. Fluid was also added between pressing cycles of cold-pressed samples. Although most of the added fluid is lost during cold pressing, some fluid is apparently present at this stage as films along grain interfaces, and also in intergranular pores. To produce wet samples without cold pressing, ground biphenyl was mixed with fluid to form a slurry that was placed between glass plates.

Cold pressing of dry and wet samples was conducted in a hand-driven hydraulic press at pressures to 170 MPa. Samples were placed between plastic sheets (250 μm thick) to prevent samples sticking to the steel anvils of the pressing assembly. Between pressing cycles (usually four), sample disks were thinned by scraping with a razor blade. Samples with an average thickness of 200 μm were next placed between glass slides.

All samples were hot-pressed in an incubator at approximately 65°C for as long as a week. Relatively long hot pressing periods are required to allow for grain growth and for annihilation of fractures that formed in the sample during cold pressing. Samples were contained in a chamber similar to that of the deformation apparatus, but without a see-through window. This technique was developed because hot pressing of test samples in the deformation apparatus had led to smaller grain sizes in the center of the see-through window than in other areas. Samples that were heat treated in the incubator mainly had short prismatic grains, however some platy grains grew as well. After initial hot pressing, samples were slowly cooled to room temperature and loaded into the deformation apparatus. To annihilate any fractures that may have been induced during sample reloading, samples were hot pressed in the deformation apparatus for ≈ 24 h.

The glass plates that confine the thin specimen sheet have frosted grips to hold the edges of the sample in place during shearing. Grain growth during hot pressing bonds the

Table 1
Conditions for simple shear experiments

Run	Preparation method	Displacement rate (mm h^{-1})	Bulk strain rate (2 mm szw[a]) (s^{-1})	T (°C)	T_h	Fluid composition	Fracture network
26	Cold pressed	1/24	5.8×10^{-6}	60	0.97	25 vol% methanol + 75 vol% H_2O	Backbone fracture network, spans szw[a]
33	Slurry	1/24	5.8×10^{-6}	50	0.94	25 vol% methanol + 75 vol% H_2O	Backbone fracture network, spans szw[a]
34	Cold pressed	1/24	5.8×10^{-6}	60	0.97	Prepared dry, some fluid present	Isolated fractures, jogs
37	Cold pressed	1/24	5.8×10^{-6}	20	0.85	25 vol% methanol + 75 vol% H_2O	Continuous fault zone subparallel frosted grip
20	Cold pressed	1/3	4.6×10^{-5}	60	0.97	H_2O	Stairstepping fracture systems
30	Cold pressed	1/3	4.6×10^{-5}	60	0.97	25 vol% methanol + 75 vol% H_2O	Stairstepping fracture systems
35	Slurry	4	5.6×10^{-4}	60	0.97	50 vol% methanol + 50 vol% H_2O	Continuous fault zone subparallel frosted grip
38	Cold pressed	4	5.6×10^{-4}	60	0.97	25 vol% methanol + 75 vol% H_2O	Continuous fault zone subparallel frosted grip

[a] szw = shear zone width.

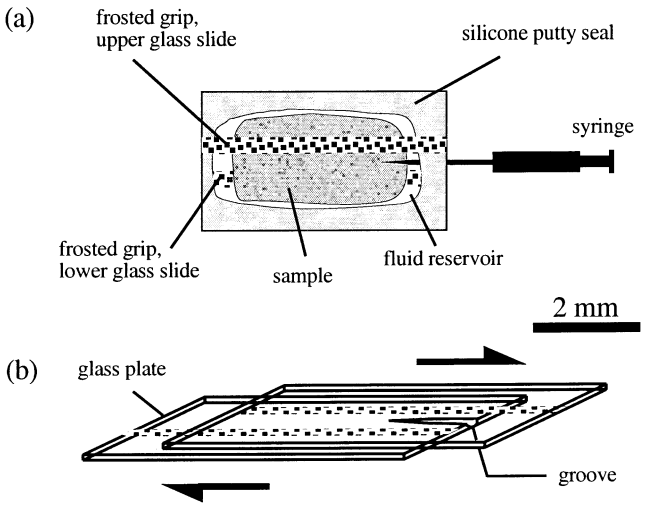

Fig. 1. Schematic sketch of sample configuration. (a) Map view of undeformed sample and specimen chamber. (b) Side view of glass slides after shear displacement. Movement of the top glass slide to the right relative to the fixed bottom glass slide produces dextral translation in the specimen volume between the frosted grips because the sample adheres to the top and bottom slides only in the areas of the frosted grips.

sample firmly to the frosted grips, such that a 2-mm-wide shear zone can develop between these predefined shear zone boundaries during shearing. Prior to sample preparation, areas between the frosted grips were coated with silicone oil to permit sliding of the sample in these areas. The glass plates were next heat treated at approximately 425°C for at least 1 h to solidify the silicone oil. The lower glass plate has a groove on one end to allow the insertion of a thin, hypodermic needle (≤400 μm thick) for injecting pore fluid during shear deformation (Fig. 1).

Fluids were, to some extent, prevented from escaping during hot pressing and deformation from all wet samples by sealing the glass–specimen–glass sandwich with a high viscosity silicone putty (Fig. 1). During hot pressing a fluid reservoir was located around the sample (Fig. 1). Biphenyl is practically insoluble in water and it is readily soluble in alcohol, even at room temperature. It is moderately volatile at the annealing temperature (65°C), and experimental temperatures of 50–60°C.

Biphenyl vapor is a powerful irritant by inhalation in humans, so sample preparation was conducted in a fume cupboard and protective clothing was worn. Hot pressing

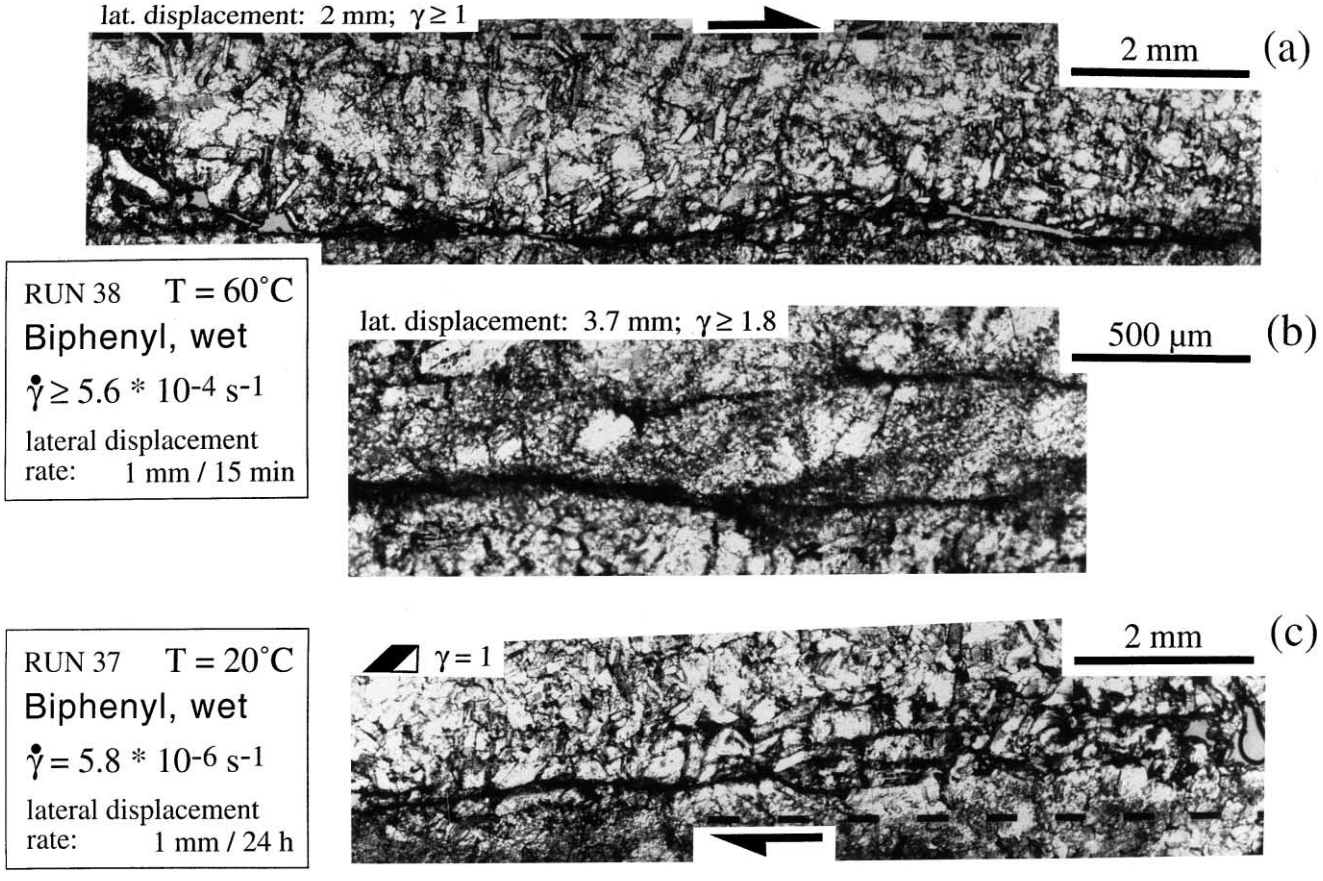

Fig. 2. Similar fault zones in two experiments conducted under different conditions. (a) Narrow fault zone after 2 mm displacement at 60°C at a displacement rate of 1 mm/15 min, (b) enlargement of the central segment of the fault zone shown above at a lateral displacement of 3.7 mm. Note the fine recrystallized grain size and the oblique grain-shape fabric in the compressional stepover. (c) A fault zone similar to that above develops at 20°C and a displacement rate of 1 mm/24 h. Broken bars indicate frosted grips.

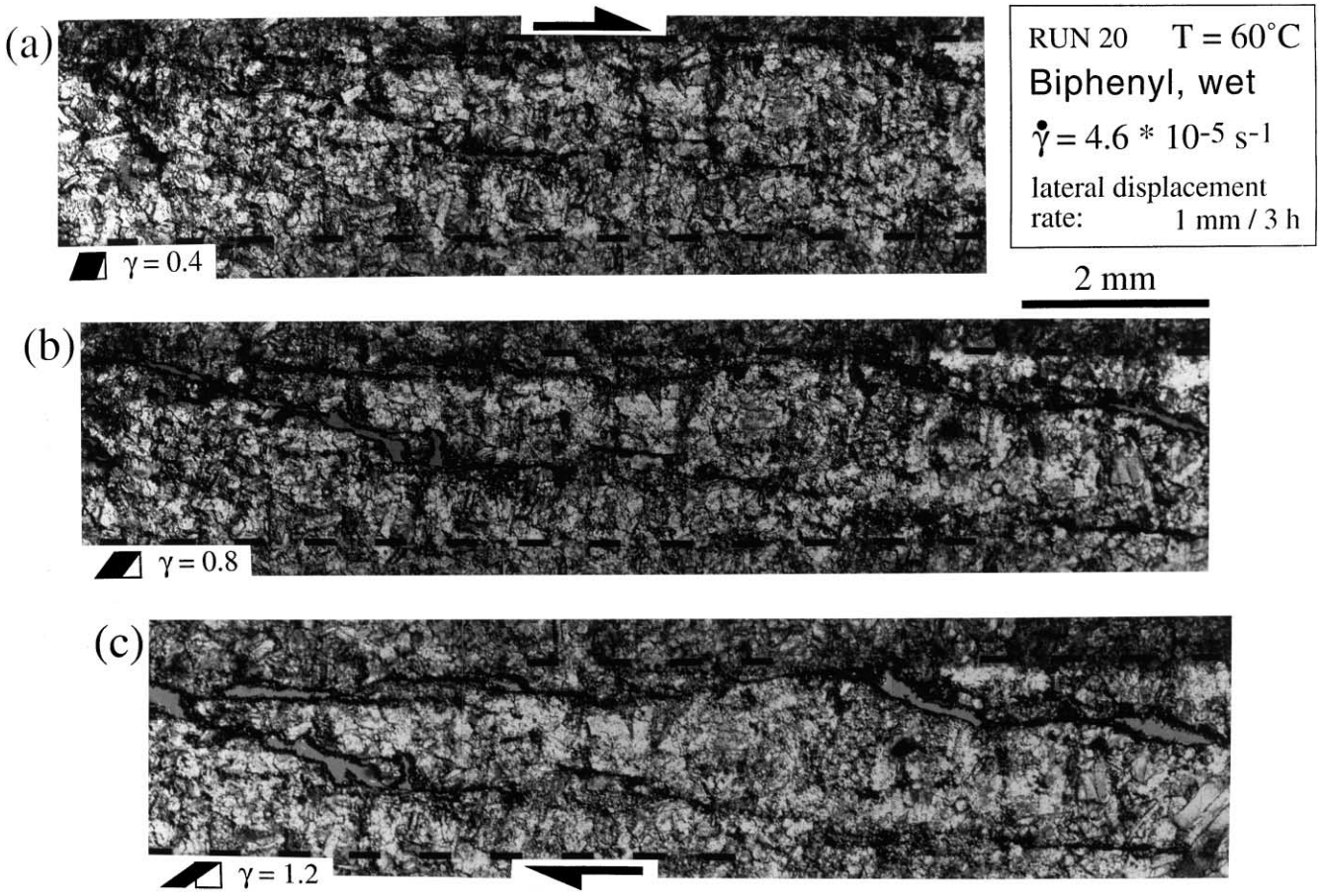

Fig. 3. Fabric evolution during shearing at 60° and a lateral displacement rate of 1 mm/3 h. Note the presence of open fractures in (b) at bulk shear strain of $\gamma = 0.8$, and in (c) the crystals that have grown into open fractures. Broken bars indicate frosted grips.

of samples, as well as shear deformation were conducted under permanent fume extraction and laboratory ventilation.

Starting materials have nearly random crystallographic and grain shape orientations and grain diameters are usually less than 500 μm. The average grain size is approximately 100 μm. Sample porosities after hot pressing were estimated visually and may only serve as a rough guide. Intergranular porosity is less than approximately 5%; pore fluid is present in intergranular pores, as well as in intragranular inclusions, which have diameters up to 30 μm. The latter form approximately 2–3% of the specimen volume.

Additional fluid was injected into the specimen assembly and fluid reservoir during deformation when connected fracture permeability was established. Injection of biphenyl-undersaturated fluid was repeated approximately once a day. Injection of alcohol–water mixtures led to dissolution of asperities along fracture surfaces at the fluid inlet; dissolution is not apparent after several minutes. Fluid pressures slightly above atmospheric pressure were attained as fluid was forced to leak along the interface between the needle and the silicone-putty seal. The silicone-putty seal formed a confining medium at approximately atmospheric pressure in the plane of the glass slides. Low stresses were applied normal to the glass slides by affixing the lid of the sample chamber finger-tight with thumb screws. Guiding steel blocks constrain relative movement of the upper and lower glass slide to produce approximately simple shear deformation.

During deformation experiments, fabric evolution in the samples was monitored by recording images with a digital video camera to produce time-lapse movies. Additional images were recorded with a 35 mm still camera, for example, to produce overviews over entire shear zones (Figs. 2–5). These images were digitized to produce fracture maps (e.g. Fig. 6) by tracing open fractures on a computer monitor. Quantitative analyses of fracture density, fracture orientation and fracture length were performed by utilizing public domain software for image analysis (NIH Image, developed at the U.S. National Institutes of Health and available on the Internet at http://rsb.info.nih.gov/nih-image/).

To investigate how fracture growth and development of fracture connectivity depends on the environmental conditions, experiments were conducted at a range of strain rates, temperatures and fluid conditions, all listed in Table 1. All samples were subjected to dextral shear. The temperature measured by the thermocouple and displayed by the control unit was tested in the range of 17–30°C. Water

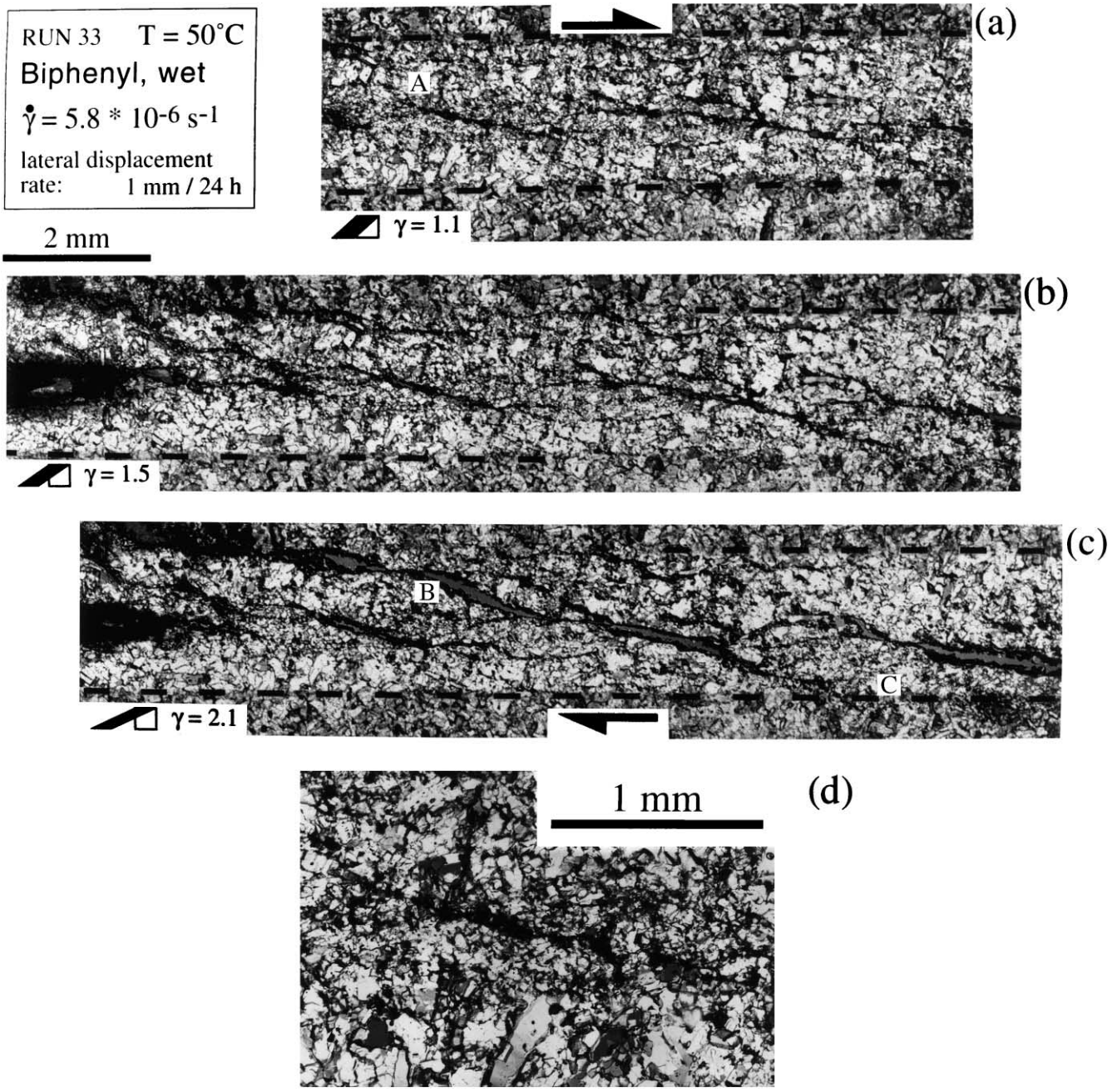

Fig. 4. Fabric evolution during shearing at 50° and a lateral displacement rate of 1 mm/24 h. (a), (b) Fractures concentrate in the middle of the shear zone and are associated with grainsize reduction in their vicinity. (c) Open fractures with lenticular shapes are linked at a bulk shear strain of $\gamma = 2.1$ to form connected fracture porosity across the shear zone. The large, open fracture segment labelled 'B' has formed at $\gamma > 1.5$. 'C' marks oblique grain-shape fabric in a zone of grain size reduction in a compressional stepover between overlapping fault segments. Broken bars in (a)–(c) indicate frosted grips. (d) Enlargement of a fracture labelled 'A' in (a). The fracture is embedded in a zone of grain size reduction with a weakly developed oblique grain-shape fabric.

was circulated through the flow conduits of the deformation apparatus during operation of the heating units. The temperature displayed by the control unit deviated by ±1°C from the outlet water temperature measured with a laboratory (mercury) thermometer. In melt experiments the displayed temperature of the control unit deviated by up to ±1°C from the nominal melt temperature of biphenyl (70°C).

3. Experimental results

Simultaneous fracturing and viscous deformation (sensu Schmid and Handy, 1991) was observed in all experiments. Viscous deformation processes include, for example, dislocation creep, diffusional mass transfer, and viscous grain boundary sliding. Open fractures are readily recognizable in the experiments because the fluid fill usually

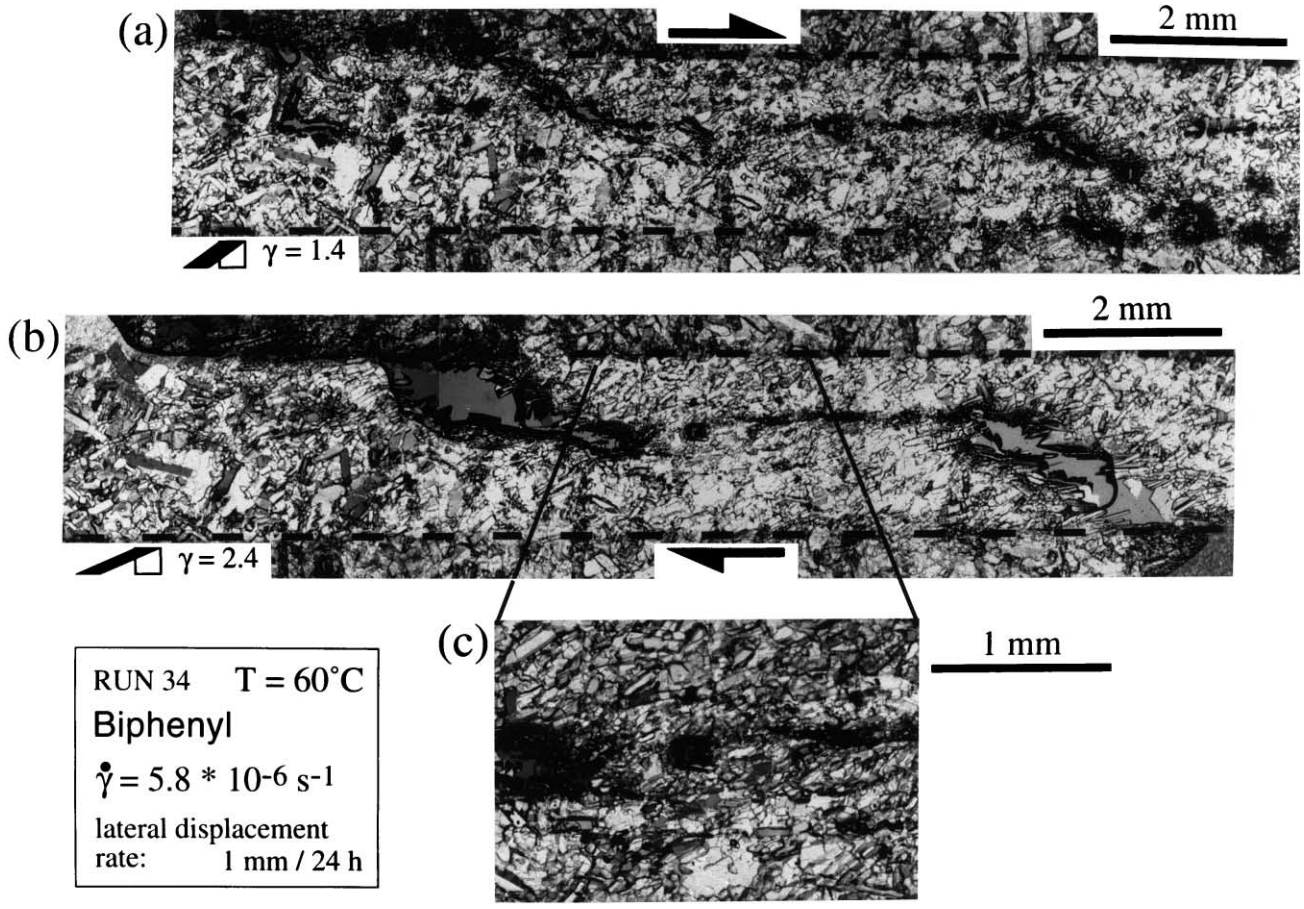

Fig. 5. Fabric evolution during shearing at 60°C and at a lateral displacement rate of 1 mm/24 h in a sample prepared dry. Although some fractures form, the bulk of the sample deforms by viscous deformation processes. An oblique grain-shape fabric develops with increasing shear strain. Note that some fractures seen in (a), as for example on the left side of the sample, become obliterated due to dynamic recrystallization at higher shear strains (b). Black-rimmed bubbles in (b) in open fractures are gas-filled. (c) Enlargement of central segment of shear zone with strongly developed oblique recrystallized grain-shape fabric. Broken bars indicate frosted grips.

contains a large proportion of vapor. The vapor component forms a dark rim at its contact with the solid phase. Thus, minute cracks appear black, and in widely open ($\geqq 20$ μm) cracks vapor bubbles show black rims.

Phase transitions were rarely observed. However, in some cases prismatic grains formed in a jerky manner within large platy grains, or platy grains spontaneously grew at the expense of nearby tabular and prismatic grains. Phase transitions were abundant in samples containing ethanol (25%)-water mixtures as the fluid phase. Results from these experiments are not described here.

In some experiments, the part of the sample between the frosted grips stuck to the upper or lower glass plate during deformation. This led to detachment of the sample from the frosted grips, easily recognizable by the many air bubbles that rapidly migrated into the area of the frosted grip. In cases where only part of the sample stuck to a glass plate, this part of the sample became disconnected from the remaining part by a fracture oriented perpendicular to the displacement direction of the upper glass plate. Again, air bubbles migrated into the frosted grip area where the sample part had detached. The rapidly appearing air bubbles in these experiments indicated that the silicone putty seal between the glass plates had ruptured. These experiments were terminated and are not presented here.

In the experiments conducted at 50–60°C, the development of microstructures at the fast strain rate is markedly different from that at the intermediate and slow strain rates. Thus, the fault zone evolution is first described at the fast strain rate, and then at the intermediate and slow strain rates. Differences in fracture evolution resulting from the deformation of nominally dry, wet and cold pressed samples, and healed slurry are described later.

3.1. Fast strain rate experiments, wet

In fast strain rate (5.6×10^{-4} s^{-1}) experiments (RUNs 35 and 38) conducted at 60°C, we distinguish between: (1) the development of fractures that are distributed over the 2-mm-wide shear zone during initial shearing, and (2) subsequent shearing along a narrow fault zone that forms at the shear zone boundary (SZB). During initial shearing ($\gamma \leq 0.3$)

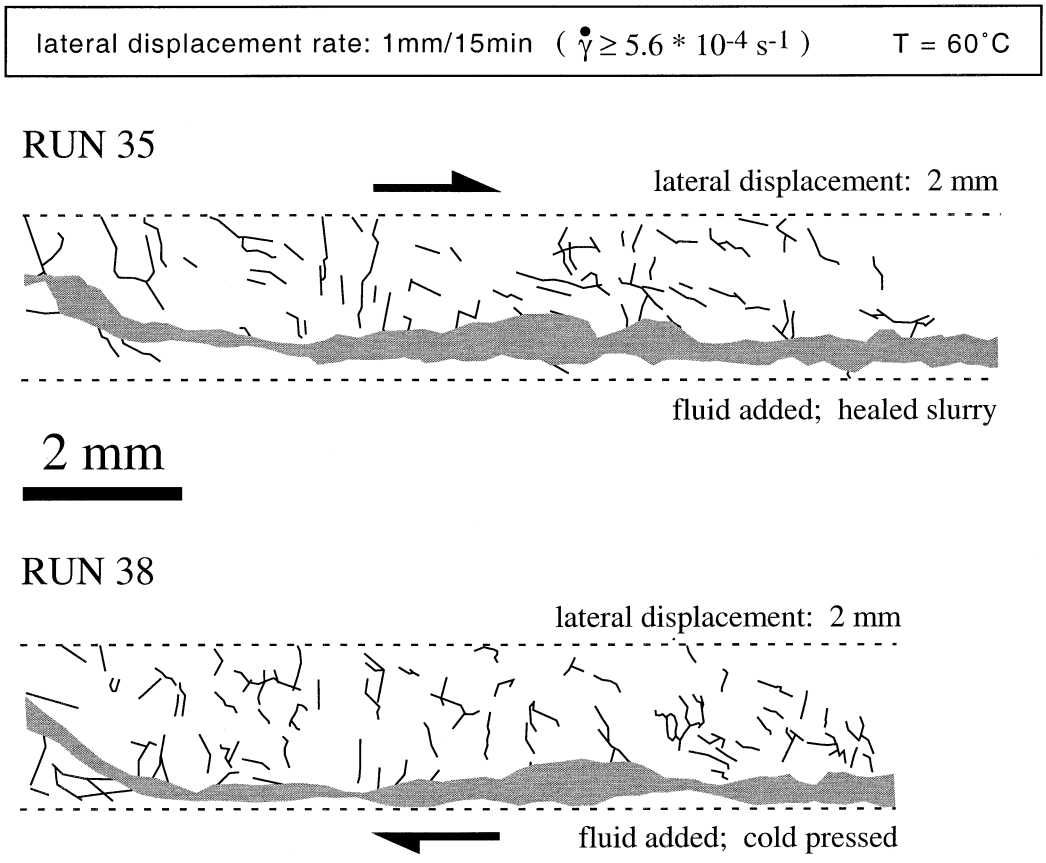

Fig. 6. Schematic sketch of fault zones (up to 0.5 mm wide) and fractures outside these fault zones in two samples deformed at 60°C and a lateral displacement rate of 1 mm/15 min. Fractures with lengths <20 μm are not shown. The sketch for RUN 38 corresponds to the shear zone shown in Fig. 2a.

fractures form predominantly at angles between 20 and 40° clockwise to the SZB. The fractures are up to 0.5 mm long. Progressive shearing leads to the localization of fracturing along one of the predefined shear zone boundaries, commonly adjacent to the edge of the frosted grip of the upper, moving glass plate. The fractures that localize at the SZB anastomose around grain aggregates and localize most of the subsequent shear deformation. By a bulk shear strain of $\gamma \approx 1$, a nearly continuous fault zone at the SZB is up to ≈ 0.5 mm wide and consists of anastomosing shear fractures, compressional stepovers and dilational jogs (Fig. 2a). Further displacement occurs predominantly along this fault zone, and subsequent strain within other parts of the sample is negligible. Although shear displacement is predominantly accommodated by sliding along fractures and dilation of fractures, shearing in compressional stepovers largely occurs by viscous processes. Continuous recrystallization transforms core mantle structures to fine-grained aggregates with oblique grain-shape fabrics (Fig. 2b). Some grain boundary sliding was observed in fine-grained aggregates.

It is noteworthy that the narrow fault oriented subparallel to the SZB usually curves into an extensional fracture inclined at $\approx 45°$ to the SZB (Fig. 2a). This extensional wing crack forms near the edge of the see-through window that lies opposite to the ram that pushes the upper glass slide. This is also the side where the lower glass plate has a groove for the insertion of a needle. This apparently is sufficient to produce a heterogeneous fracture geometry in these fast strain rate experiments. On the other side where the ram pushes the upper slide, the trace of the fault zone continues in a nearly straight line to the edge of the see-through window.

3.2. Intermediate and slow strain rate experiments

3.2.1. Low temperature (20°C) experiment, wet

A continuous fault zone developed along one of the shear zone boundaries during shearing of a wet sample (RUN 37) at the slowest strain rate ($5.8 \times 10^{-6}\ s^{-1}$) and a temperature of 20°C (Fig. 2c). It may be noted that the local strain rate in the fault zone is higher than the bulk strain rate imposed on the sample. Fracturing in other parts of the sample is very limited between the frosted grips, leaving a large proportion of the sample within the 2-mm-wide zone undeformed. By a displacement of 2 mm, the fault zone is approximately 0.5 mm wide and consists of anastomosing shear fracture networks similar to those formed during fast shearing at 60°C (see Fig. 2a, RUN 38), and described in the previous section. Grain size reduction occurs in the direct vicinity of

faults, and in particular in compressional stepovers. The development of core-mantle structures in grains in compressional stepovers, weakly developed oblique recrystallized grain-shape fabrics, and observed grain boundary migration indicate that dislocation flow occurs together with brittle process at 20°C ($T_h = 0.85$).

3.2.2. High temperature (50–60°C) experiments, wet

At high temperatures and intermediate ($4.6 \times 10^{-5}\ s^{-1}$) and slow ($5.8 \times 10^{-6}\ s^{-1}$) strain rates (RUNs 20, 30 and 26, 33) we distinguish between two stages of fault zone evolution. In the first stage, during initial shearing, isolated fractures form. In a second stage, during progressive shearing, fractures grow and stairstep across large parts of the shear zone. At the slowest strain rate, fractures form connected fracture systems linking opposite sides of the shear zone. Fault zone evolution is similar in these wet samples whether they were cold pressed or not.

During initial shearing, many fractures form at angles of 20–50° to the SZB in wet samples (Figs. 3a and 4a) and have lengths between 1 and 2.5 mm. At the slowest bulk strain rate ($5.8 \times 10^{-6}\ s^{-1}$) fractures are concentrated in the middle of the shear zone (Fig. 4a and b). However, some fractures do form near the SZB at the intermediate and slowest strain rates. Despite slip and dilation along fractures, parts of the samples deform by viscous deformation processes. Even during initial shearing, fractures are usually associated with grain size reduction in their direct vicinity (Fig. 4d). Fine-grained aggregates contain weakly developed oblique grain shape fabrics. Grain boundary migration with bulging of grain boundaries is commonly observed and indicates that dislocation flow occurs as a viscous deformation process.

During progressive shearing, linked fracture systems develop by further growth of pre-existing fractures. Such fracture linkage can, for example, be seen between bulk strains of $\gamma = 1.5$ and $\gamma = 2.1$ in RUN 33. A fracture segment (B in Fig. 4c) with an orientation oblique to the SZB connects previously unconnected fractures. This connecting fracture is open at $\gamma = 2.1$. Displacement along fracture segments with orientations subparallel to the SZB can lead to opening of fracture segments that enclose angles of $\geqq 20°$ with the SZB (Figs. 3 and 4). Open fractures then form stairstep-linked trails of dilatant jogs with lenticular to sigmoidal shapes. The length of jogs in linked fault-jog systems is typically 1–2 mm. One or more linked fault-jog systems may develop within the bulk shear zones, localizing most of the subsequent displacement. However, overlapping fault segments that form compressional stepovers (e.g. C in Fig. 4c) tend not to be completely connected by fractures. Slip transfer in these sites is predominantly facilitated by viscous deformation processes. Grain boundary migration is observed in compressional stepovers where oblique grain-shape fabrics develop in fine-grained aggregates.

Once fracture systems are connected, such that displacement localizes along fractures subparallel to the SZB, further deformation does not usually cause significant changes in the overall shear zone geometry. Nearly stable fracture geometries were attained at a bulk shear strain of $\gamma \approx 0.8$ at the intermediate strain rate and at a bulk shear strain of $\gamma \approx 2$ at the slowest strain rate. Experiments were terminated at bulk shear strains of $\gamma \approx 3$–4.

3.2.3. Shearing of a sample prepared without added fluid (60°C)

Deformation of a nominally dry sample (RUN 34) at the slowest strain rate ($5.8 \times 10^{-6}\ s^{-1}$) occurred predominantly by viscous deformation processes. The development of an oblique grain-shape fabric (Fig. 5) together with observed grain boundary migration indicate dynamic recrystallization during dislocation flow processes. The oblique grain shape fabric is similar to those found in many naturally deformed quartz mylonites (e.g. Lister and Snoke, 1984; Law, 1998) and in shear experiments on other dry rock analog materials (e.g. Herwegh and Handy, 1996, 1998). The grain-shape fabric in this experiment forms an angle of 25–35° to the SZB. Some low angle fractures also developed during initial shearing as in the wet experiments described above. Progressive shearing led to the development of two jogs with left-stepping en échelon geometry due to dilation of fractures that initially were inclined at 45° to the SZB (Fig. 5). During progressive shearing, strain localizes between these jogs in the middle of the shear zone by viscous deformation processes. Strain also localizes where jogs contact shear zone boundaries. As can be seen from Fig. 5a and b, the open fractures in RUN 34 contain two separate vapor and liquid phases. The liquid phase is likely to be silicone oil released from the silicone sealant. The liquid that bounds the large vapor bubble in the bottom right hand corner in Fig. 5b is, in fact, silicone sealant that has intruded from the sample edge into the jog. Vapor bubbles are inferred to contain air trapped during sample preparation, as well as vaporized biphenyl.

4. Evolution of fracture networks

Markedly different fracture geometries developed in experiments conducted at different strain rates. Changes in temperature and fluid content have also influenced the microstructural evolution of the sample shear zones. To quantify some of the differences observed during the evolution of fracture systems, fracture connectivity and fracture densities were mapped in several experimental shear zones. Fractures with lengths less than 200 μm were not considered, as these are difficult to image during experiments.

Growth of blocky to prismatic grains from the jog walls into pore space occurred during deformation in all experiments, regardless of whether or not fluid was added during sample preparation. Crystal growth in pore spaces occurs from either liquid pore fluid or vapor. The growth direction

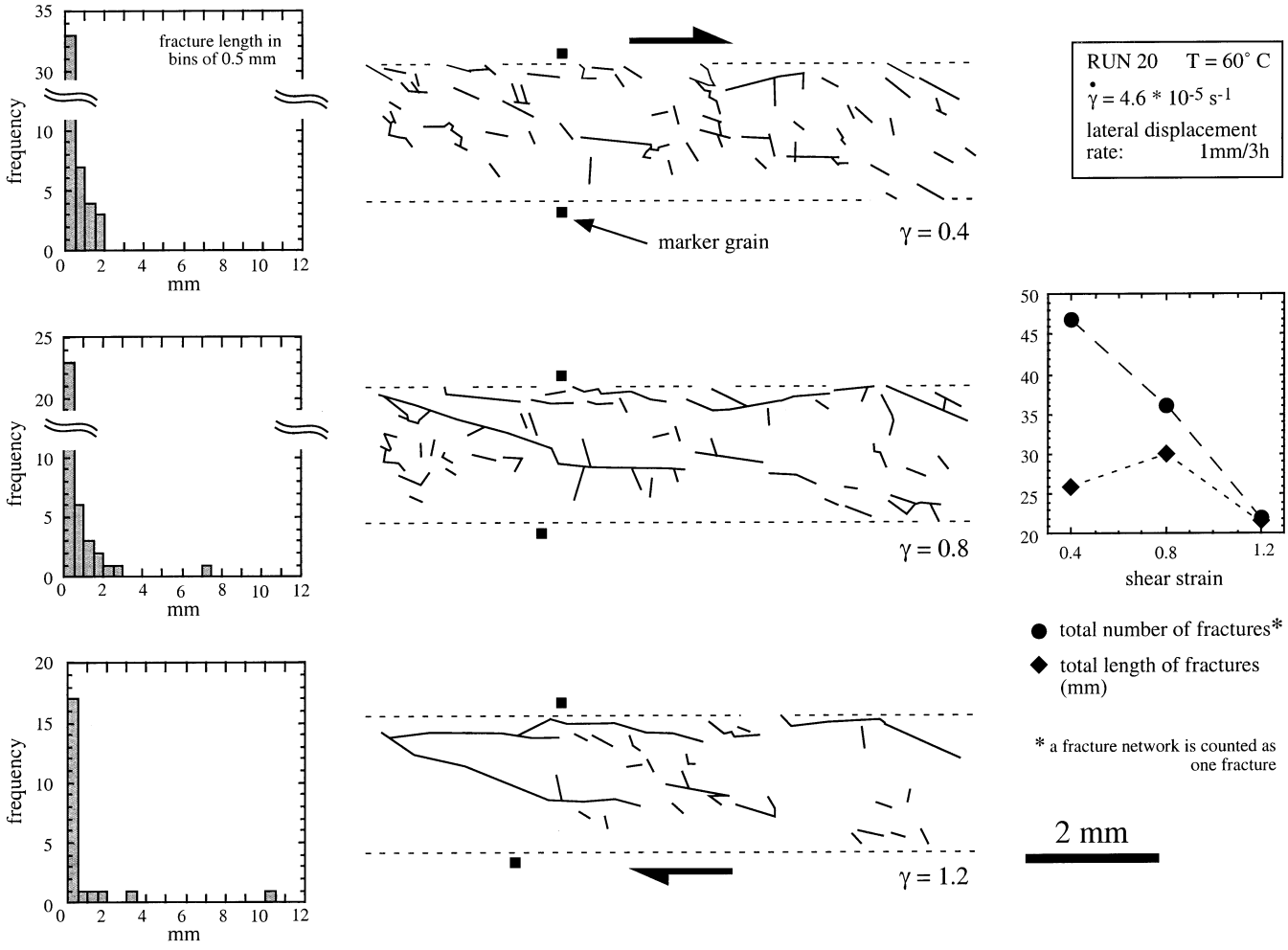

Fig. 7. Fracture distributions at different shear strains for RUN 20 conducted at the intermediate bulk strain rate. The fracture maps of equal area correspond to the shear zones shown in Fig. 3. Fracture length is traced omitting fractures with lengths of less than 200 μm. The distributions of fracture lengths are plotted in histograms for each strain increment shown. The total number and length of fractures are also plotted as a function of bulk shear strain.

of these crystals is predominantly subperpendicular to the jog or fracture walls (Figs. 3 and 4). This orientation also mimics the substrate grain orientation in cases where fracture walls have grains with an oblique shape fabric. Interaction of asperities on fracture surfaces during progressive shearing of biphenyl is described by Streit and Cox (2000).

4.1. Fracture connectivity

The fracture connectivity attained outside the continuous fault zone in fast strain rate experiments (RUNs 35 and 38) at a lateral displacement of 2 mm is schematically shown in Fig. 6. Fractures apparently do not connect across the 2-mm-wide shear zone defined by the frosted grips. Although prominent fracture connectivity exists within the fault zone subparallel to one of the frosted grips, connectivity is not necessarily continuous as shearing in compressional stepovers (Fig. 2b) occurs by viscous deformation processes.

The evolution of fracture connectivity with increasing strain has been examined in detail for two experiments conducted at the intermediate (Fig. 7) and the slow strain rates (Fig. 8). Isolated fractures and fracture networks were mapped and their fracture length was measured using a computer imaging program (NIH-Image). Again, fractures with lengths less than 200 μm were not considered, as these are difficult to image during experiments, and because errors in length measurement are large for small fractures. In both experiments (RUNs 20 and 33) the evolution of fracture networks is similar. Increasing strain leads to the development of several linked fracture networks. The number of relatively short fractures decreases with increasing strain due to fracture linkage and due to sealing-healing processes (compare Figs. 7 and 8). These processes include fracture closure due to material diffusion and compression normal to fracture walls, followed by elimination of intergranular fracture planes by dynamic recrystallization. Both of the above experiments indicate that the total number of open fractures decreases with increasing strain after a maximum value is attained (Figs. 7 and 8). In addition, the total length of all

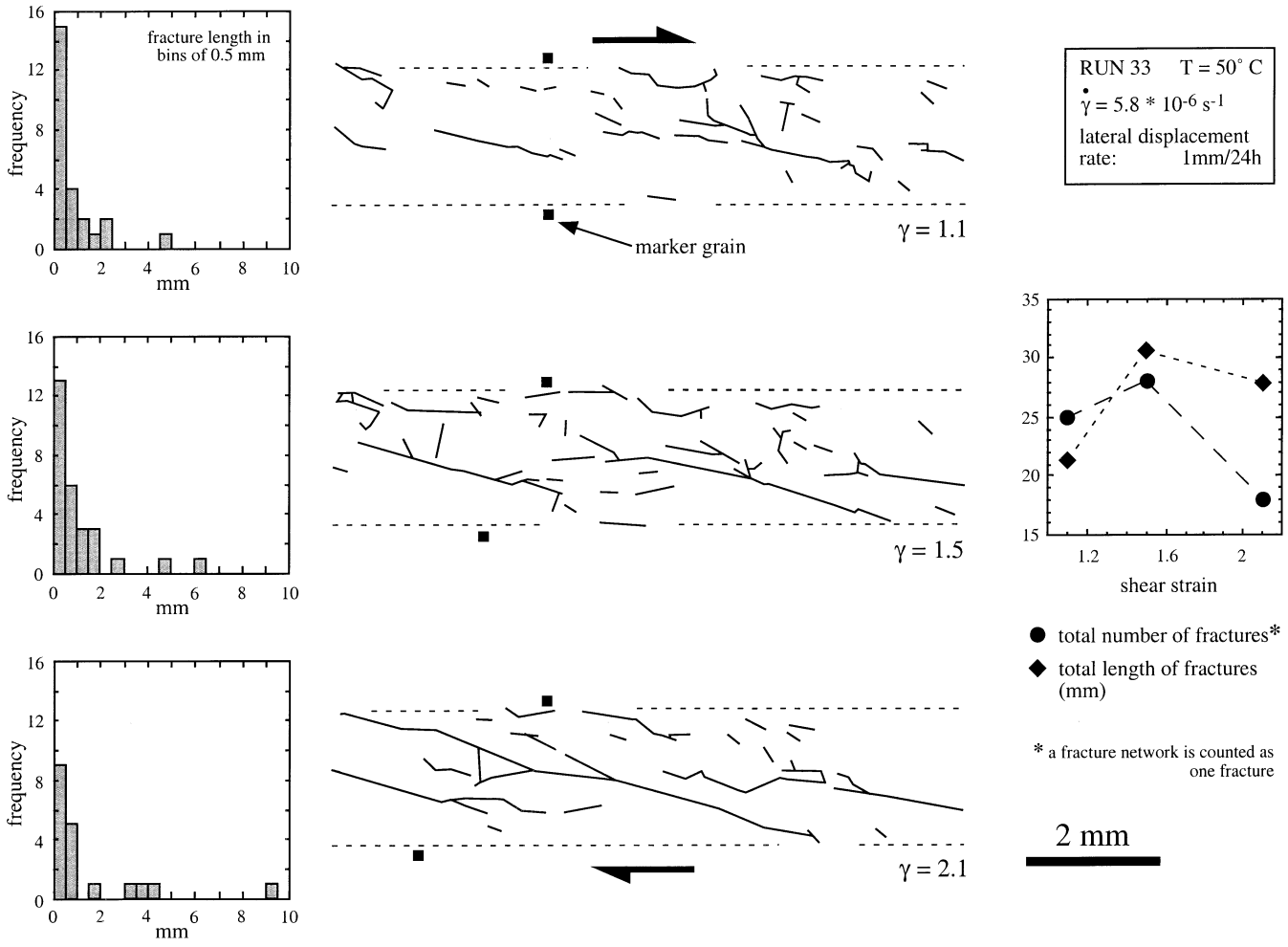

Fig. 8. Fracture distributions at different shear strains for RUN 33 conducted at the slowest bulk strain rate. The fracture maps of equal area correspond to the shear zones shown in Fig. 4. Fracture length is traced omitting fractures with lengths of less than 200 μm. The distributions of fracture lengths are plotted in histograms for each strain increment shown. The total number and length of fractures are also plotted as a function of bulk shear strain.

fractures and fracture systems apparently decreases towards higher strains after a peak value is attained, as is shown in Figs. 7 and 8.

4.2. Fracture distribution and connectivity as a function of pore fluid presence

The distribution of fractures and the evolution of fracture networks is compared in experiments conducted on hot-pressed samples prepared from starting aggregates which were: (1) nominally dry, (2) wet and cold-pressed, and (3) a wet slurry. The samples were deformed at the slowest bulk strain rate ($5.8 \times 10^{-6}\ s^{-1}$) and at similar temperatures (50–60°C). As seen from Fig. 9, the two experiments (RUNs 33 and 26) on wet samples have higher areal fracture densities (>1.3 mm mm^{-2}) than the experiment (RUN 34) on the nominally dry sample (0.43 mm mm^{-2}). In the two wet samples (RUNs 26 and 33), the areal fracture density of RUN 26 (2.28 mm mm^{-2}) exceeds that of RUN 33 (1.37 mm mm^{-2}) by a factor of 1.7. The different fracture densities in these three samples are associated with the development of different fracture types.

With regard to the role of fractures in transporting fluids, three types of fractures are recognized on the basis of their connectivity in fracture systems. These are: (1) backbone fractures, which connect opposite sides of flow systems (e.g. source and sink region) and carry the bulk fluid flux, (2) dead-end fractures or dangling fractures, which branch off the backbone fractures, and (3) isolated fractures (e.g. Sahimi, 1994; Cox, 1999; Cox and Knackstedt, 1999). In the shear experiments presented here, fractures that link one side of the 2 mm shear zone to the other are termed backbone fractures. Only isolated fractures developed in the experiment (RUN 34) on the nominally dry sample (Fig. 9). These isolated fractures apparently lack branching fractures. All three fracture types are present in the experiments on wet samples (Fig. 9). Only a limited number of dangling fractures developed in RUN 33 (healed slurry) compared with the high number of dangling fractures occurring in RUN 26 (cold pressed sample).

The backbone fractures that developed in both

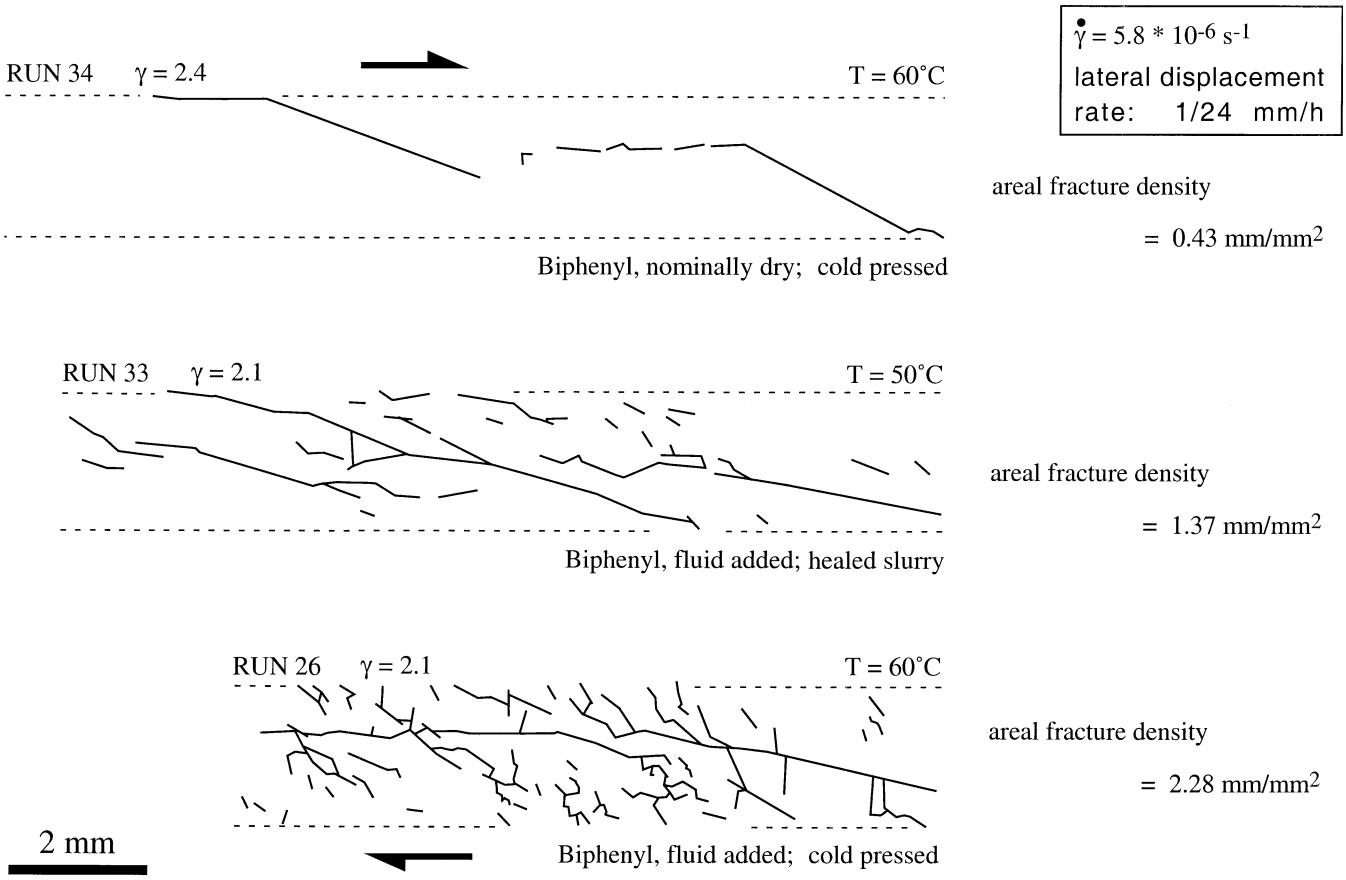

Fig. 9. Fracture maps from three experiments conducted at the slowest bulk strain rate on samples prepared dry and wet. Fracture length is traced omitting fractures with lengths of less than 200 μm. Areal fracture densities are calculated for the depicted shear zone areas. Mapped shear zone area for RUN 34 is the same as that shown in Fig. 5b, and shear zone area for RUN 33 corresponds to that shown in Fig. 4c.

experiments on wet samples (RUNs 33 and 26) have orientations oblique to the SZB, and shear displacement along these backbone fractures is synthetic with respect to the overall shear sense. The backbone fractures enclose, on average, angles of 10–20° with the SZB.

5. Discussion

Experiments in approximately simple shear mode on biphenyl aggregates in a see-through deformation apparatus have shown that the geometry and evolution of fracture porosity in low effective pressure regimes are strongly strain rate dependent at high homologous temperatures.

The experiments additionally indicate that the styles of fracture networks are also influenced by the presence and distribution of reactive pore fluids in samples. The microstructural evolution of the grain aggregates, in particular the evolution of fracture connectivity and strain localization, are discussed below in terms of strain rate and effective confining pressure effects on partitioning of strain between viscous and brittle processes. The implications of strain dependent crack connectivity for the evolution of mechanical and fluid transport properties in natural shear zones are also considered.

5.1. Fluid pressure and effective stress conditions in the experiments

The experimental set-up used does not permit precise control of confining pressure or internal pore fluid pressure. The silicone putty seal used in these experiments confines vapor formed during shearing, as well as the added pore fluid in wet samples, to the sample chamber at approximately atmospheric pressure until the seal breaks at high shear strains ($\gamma > 4$). In wet experiments, the small volume change of vapor bubbles associated with pore pressurization during fluid injection during shearing of samples, indicates that vapor pressure is nearly as high as pore liquid pressure. At least in the slow strain rate experiments at 50–60°C, vaporization of biphenyl is inferred to compensate for any fluid pressure loss due to crack growth and dilation. It is thus inferred that fluid pressures were close to confining pressure in these experiments, and that effective confining pressures were close to zero.

5.2. Effects of fluid presence on deformation processes

Fracturing and viscous deformation processes occurred in all deformed samples. However, the relative importance of these processes differs between experiments conducted at the same strain rate ($5.8 \times 10^{-6}\ s^{-1}$) and similar temperatures (50–60°C) on samples prepared nominally dry (RUN 34) and prepared wet (RUNs 26 and 33). The areal fracture density in experiments on wet samples exceeds that in a nominally dry experiment (RUN 34) by factors of 3.2–5.3 (Fig. 9). In RUN 34, displacement is predominantly accommodated by viscous deformation processes in major parts of the sample shear zone. Detailed descriptions of predominantly viscous deformation in dry rock analog materials are given by Urai et al. (1980) and Herwegh and Handy (1996, 1998). In contrast to the nominally dry experiment on biphenyl, viscous processes including dislocation flow are localized to the vicinity of fractures and to compressional stepovers between discontinuous fractures in experiments on wet samples. Evidently, the presence of fluids in biphenyl aggregates increases the importance of fracturing and sliding along fractures as a deformation process, even at high homologous temperatures.

The highest fracture density developed in RUN 26, although this run was conducted at a higher temperature (i.e. 60°C) than RUN 33 (i.e. 50°C) (Fig. 9). Shearing at a higher temperature may be expected to lead to lower fracture density, as higher temperatures usually favor viscous deformation processes (e.g. Chester, 1988). Here, the difference in areal fracture density between RUNs 33 and 26 is possibly related to a different starting porosity due to the different sample preparation techniques applied (see Table 1).

It is known from triaxial rock deformation experiments that pore fluid pressures in rocks can reduce total stresses to effective stresses and thus induce fracturing by reducing the applied confining pressure (e.g. Handin et al., 1963; Murrell, 1965). The formation of veins in shear zones is usually attributed to this effect (e.g. Etheridge, 1983). The formation of many fractures in the experiments on samples that were prepared wet and deformed at low effective confining pressure are likely to be the result of this effect.

5.3. Effects of strain rate and temperature on fracture distribution and linkage

The distribution of fractures and the geometry of fracture networks in experiments conducted on wet samples at 50–60°C is sensitive to the applied strain rate. At all applied strain rates (5.6×10^{-4}–$5.8 \times 10^{-6}\ s^{-1}$), fractures nucleate and grow throughout the 2-mm-wide zones between the frosted grips during initial shearing. At the slowest strain rate, continued fracture growth occurs over the full shear zone width during shearing up to $\gamma \approx 2$. However, at the fastest strain rate, localization of displacement within a fault zone ($\leq$0.5 mm wide) adjacent to a SZB occurs at $\gamma \approx 1$. At 20°C, and at the slowest strain rate, localization of shear displacement along a boundary fault zone occurs at lower shear strains ($\gamma \approx 0.5$). In this experiment, however, little fracturing occurred in other parts of the sample during initial shearing. Thus, shear localization occurs along fault zones near a SZB at high shear strains and strain rates at 50–60°C, and at low shear strains during the low temperature (20°C) experiment. This is consistent with sample-scale faulting induced during experimental deformation of synthetic amphibolite by decreasing the temperature or by increasing the strain rate in contrast to distributed deformation at slower strain rates and higher temperatures (Hacker and Christie, 1990). Also consistent with the development of fault zones in fast strain rate experiments on biphenyl is the localization of strain into a narrow zone in wet Hale albite rock deformed at a faster strain rate than that for homogenous deformation (Tullis and Yund, 1980).

In all experiments on wet samples, deformation drives progressive fracture nucleation and growth. Later on in the experiments, shear displacement occurs predominantly along linked fractures and fracture networks. Backbone fractures that connect opposing sides of 2-mm-wide shear zones form at relatively low shear strains ($\gamma \leq 2.1$) in experiments conducted at the slowest strain rate at 50–60°C.

Numerical modelling of the evolution of fracture connectivity in a brittle material subjected to pure shear shows that sample-spanning backbone fracture networks can be attained at even lower strains in 3D space than in 2D space (Cox and Knackstedt, 1999). The development of highly connected fracture networks at low shear strains has two important consequences. Firstly, the development of fracture connectivity will be associated with a sudden increase in fracture permeability in the shear zone. The experimental results indicate that, even at high homologous temperatures, the permeability evolution of shear zones is sensitive to strain, effectively confining pressure and strain rate. Secondly, the point in the strain history at which a backbone fracture network first forms may have important consequences for the mechanical behavior of the shear zone. Prior to the percolation threshold, distributed shear strain is achieved by mixed brittle and viscous processes. After the percolation threshold, localization of displacement and dilatation to the backbone fracture leads to a transition from mixed brittle-viscous to predominantly brittle-frictional deformation.

5.4. Dynamic competition between fracture growth and closure

Disappearance of some fractures with lengths $\geqq 200\ \mu m$ with increasing strain is evident from fracture maps created from RUNs 20 and 33 (Figs. 7 and 8). These experiments were conducted on wet samples at 50–60°C at intermediate and slow strain rates. The number of recorded fractures decreases in both experiments towards higher strains and is partly due to the linkage of fractures. However, the

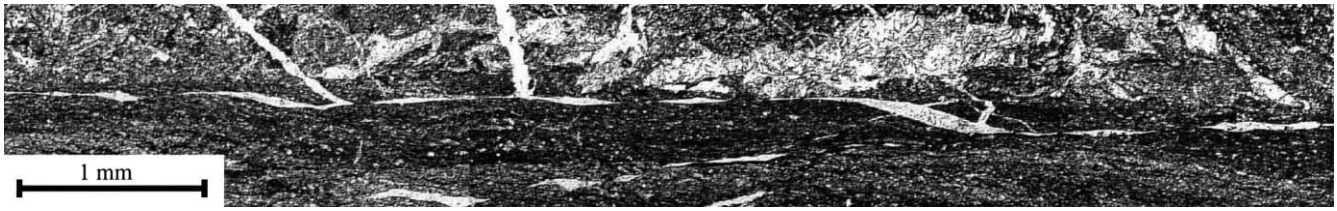

Fig. 10. Linked stairstepping vein system in foliated cataclasite. The veins are predominantly filled with chlorite and occasionally some epidote. In the larger lenticular veins oriented obliquely to the foliation of the cataclasite, the chlorite filling has a weak foliation parallel to the vein orientation. Epidote vein fillings (not in field of view) have undulose extinction. The cataclasite has formed in a greenschist body and consists mainly of epidote, titanite, albite and chlorite. Note that the linked vein system spans a reactivated cataclasite (dark grey) with finer grain size and different composition than older host cataclasites.

decrease of the total length over all fractures and fracture networks recorded at $\gamma > 0.8$ in RUN 20 and at $\gamma > 1.5$ in RUN 33 indicates that some fractures disappear or reduce in length below the limit of recording (i.e. <200 μm long). Although fracture growth is dominant over fracture closure at low shear strains, fracture closure becomes more important when fracture linkage leads to localization of shear displacement along fracture networks. This trend indicates that progressive shearing at high homologous temperatures and a slow strain rate leads to localization of fracture porosity and shear displacement along connected fracture networks.

5.5. Fracture geometries and networks in experimental and natural shear zones

The orientation of backbone fractures produced in some experiments is similar to the orientation of synthetically oriented Riedel shears (R1) observed in natural and synthetic fault gouges, as well as sheared sands and other materials (e.g. Logan et al., 1992, and references therein). It is probably the most prominent fracture orientation in natural fracture systems at a millimetre to kilometre-scale (e.g. Tchalenko, 1970; Swanson, 1988; Takagi, 1998).

The shapes of open fracture segments, especially in the intermediate and slow bulk strain rate experiments, resemble lenticular veins and jogs in natural shear zones that have not undergone significant deformation after vein or jog formation (e.g. Kerrich and Allison, 1978; Stel, 1981; Sibson, 1985; Nguyen et al., 1998). Analogies to the stair-step-linked jogs and fractures (e.g. Figs. 3c and 4c), which form backbone fracture porosity in some of the slow strain rate experiments (Figs. 4c and 9), can also be found in natural shear zones. Fig. 10 depicts stairstep-linked chlorite veins that span a foliated cataclasite that consists of fine-grained epidote, albite, titanite and chlorite. This cataclasite has formed in a 40–60-m-wide lower greenschist facies shear zone (Streit, 1998). The lenticular veins in the cataclasite have the same geometry and orientation as those produced in our slow strain rate experiments under fluid saturated conditions (RUNs 33 and 26). The scale of the natural example is similar to the experimental scale.

5.6. Brittle-viscous deformation in experimental and natural shear zones

The operation of both brittle and viscous deformation processes in the experimental shear zones suggests that the shear zone behavior is similar to that of some mid-crustal shear zones (e.g. O'Hara, 1990; de Roo and Williams, 1990; Streit and Cox, 1998). Additionally, the discontinuous fault zones that form both during fast ($5.6 \times 10^{-4}\,s^{-1}$) and slow ($5.8 \times 10^{-6}\,s^{-1}$) shearing by fracturing in conjunction with viscous deformation in compressional stepovers, are analogous to some natural fault systems that exhibit transitions between brittle and viscous behavior along their length. For example, Bürgmann and Pollard (1994) described discontinuous strike-slip faults with plastic deformation and dynamic recrystallization of quartz, and the development of S–C type fabrics localized in compressional stepovers, whereas brittle deformation associated with vein development is localized in extensional stepovers. Simultaneous viscous deformation and fracturing also occurs in deep crustal shear zones that contain melt (Handy and Streit, 1999).

5.7. Inferences from analog experiments for natural shear zones

The experimental results on analog materials provide insights into deformation processes and their dependence on fluid activity in natural shear zones. The presence of reactive pore fluids at pressures close to experimental confining pressures may simulate low effective confining pressures in some natural shear zones. Low effective confining pressures, or near-lithostatic fluid pressures are expected to develop where active shear zones and faults localize high fluxes of hydrothermal fluids (Streit, 1997, and references therein); these structures are prevalent in deforming and prograding metamorphic rocks at mid to deep crustal levels (e.g. Etheridge et al., 1983, 1984; Hickman et al., 1995).

The observation that slip tends to become localized adjacent to frosted grips with increasing imposed shear strain rate, increasing shear strain, and decreasing temperature suggests that shear displacement at near seismic slip velocities is likely to localize along pre-existing anisotropies at high strains. Such anisotropies, similar to the

frosted grips in our experiments, may include competence contrasts, metamorphic layering, foliations, veins or pre-existing faults.

In the analog-material experiments, fractures form mm-scale networks distributed across 2 mm shear zone width only in the slow strain rate, high temperature, wet experiments. Similar, pervasive fracturing may develop in medium to high grade metamorphic shear zones in fluid active regimes. The development of highly interconnected fracture networks in the experimental shear zones requires the presence of added pore fluids, which are inferred to be at pressures close to confining pressure. In natural shear zones, pervasive grain-scale fluid penetration of the shear zone matrix via extensive fracture networks is likely to be influenced by infiltration of fluids at pressures close to lithostatic.

In the experimental shear zones, the development of highly connected fracture networks at relatively low bulk strains ($\gamma \leq 2.1$) is consistent: (1) with triaxial deformation experiments on calcite aggregates at low effective pressures (Zhang et al., 1994), and (2) with two and three-dimensional models by Cox and Knackstedt (1999). It is suggested that pervasive grain-scale fracturing and attendant high permeability can also develop in natural shear zones at relatively low shear strains. In simple shear regimes, the shear zone width and nature and localization of fracture networks within shear zones will be important factors influencing the rock volume affected by infiltrating fluid. Towards the lower crust, where shear zones tend to widen (e.g. Sibson, 1986), distributed and highly connected fracture permeability is expected to permit fluid access to, and reaction with, large volumes of deforming rock provided pore fluid factors (pore fluid pressure/overburden pressure) are high. Similarly, outside shear zones, pervasive, grain-scale fracturing and associated fluid flow in large crustal volumes, which deform at high pore fluid factors by mixed brittle-viscous mechanisms, also provide potential for fluid leaching of large quantities of precious metals. Focusing of the flow of such fluids towards narrow shear zones and faults and their delivery to higher crustal levels in active and permeable shear networks is a key factor for localizing the formation of many types of hydrothermal ore deposits (Cox, 1999). Positive feedback between fluid infiltration, fracture growth and further localization of fluid flow may potentially impact on crustal strength. This will be particularly important if fluid-driven growth of fracture networks promotes fluid infiltration and thereby decreases effective stresses and frictional strength.

6. Conclusions

The evolution of fracture networks at high homologous temperatures (0.85–0.97) was monitored during simple shear deformation of wet and nominally dry biphenyl aggregates in a see-through deformation apparatus. The presence of fluids at pressures close to the low experimental confining pressures leads to nucleation and growth of fracture networks. Viscous deformation processes operate in conjunction with fracture growth and frictional sliding, but tend to be localized in compressional stepovers between discontinuous fracture systems and in the vicinity of fractures that localize slip. These areas are usually associated with intense grain size reduction and the development of weak to moderate shape preferred orientations. In contrast, in the nominally dry sample deformed at the slowest strain rate and at 60°C, viscous deformation processes including dislocation flow are predominant and fracture growth is limited to produce some isolated fractures.

In the wet biphenyl aggregates, the evolution of fracture connectivity is strongly strain rate-dependent at 50–60°C. Fast shearing leads to the development of a narrow fault along a SZB, whereas slow shearing leads to jog and fracture arrays with stairstep-linkage across the shear zone. Sample-spanning backbone fracture arrays develop at low shear strains ($\gamma \leq 2.1$) in wet samples at the slowest strain rate. At higher strains, most deformation is localized by slip and dilatation on the backbone fracture population.

Detailed fracture analyses on wet and dry samples deformed at 50–60°C at intermediate and slow strain rates show that the number of fractures decreases with increasing strain due to fracture linkage. Although fracture growth is dominant over fracture closure during initial deformation, fracture closure becomes important during progressive shearing, even at low bulk shear strains ($\gamma \leq 0.8$). At the slowest strain rate, fracture densities in wet samples exceed that of a nominally dry sample by factors of three to five.

The geometry and orientation of fractures and fracture networks, as well as the deformation processes in the experimental shear zones, are similar to those that occur in some natural shear zones that have been exhumed from mid and deep crustal levels. Based on the experimental results, it is suggested that when pore fluid factors are high enough to drive grain-scale fracture growth, the infiltration of pressurized fluids into active shear zones can lead to rapid fracture nucleation and growth, and attendant permeability enhancement at relatively low shear strains, even at very high homologous temperatures. Grain-scale connected fracture permeability in active shear zones may therefore be very important in controlling the mechanical behavior of shear zones and the architecture of fluid flow at mid- to deep crustal levels.

Acknowledgements

J.E. Streit thanks Mark Handy, Peter Bauer and Claudio Rosenberg (University of Giessen) for numerous, inspiring discussions on shear deformation of analog materials and on the improvement of the experimental techniques. In particular Peter Bauer, Claudio Rosenberg and Marco Herwegh (University of Bern) introduced J.E.S. to the techniques of

sample preparation. Methods of wet sample preparation were developed in collaboration with Peter Bauer. Cees Passchier and Bas ten Brok are thanked for providing information on silicone putty products. Richard Bale (University of Newcastle) and Norm Fraser (ANU) provided technical assistance during laboratory set-up. Richard Barwick and Harri Kokkonen assisted with photographic reproductions. Critical reviews by M. Herwegh and J. Urai are appreciated. This research was supported by the Australian Research Council.

References

Angevine, C.L., Turcotte, D.L., Furnish, M.D., 1982. Pressure solution lithification as a mechanism for the stick-slip behavior of faults. Tectonics 1, 151–160.

Bernstein, J., Sarma, J.A.R.P., Gavezzotti, A., 1990. Generation of unknown crystal phases for aromatic hydrocarbons by packing energy calculations. Chemical Physics Letters 174, 361–368.

Boullier, A.-M., Robert, F., 1992. Palaeoseismic events recorded in Archean gold-quartz vein networks, Val d'Or, Abitibi, Quebec, Canada. Journal of Structural Geology 14, 161–179.

Brantley, S.L., 1992. The effect of fluid chemistry on quartz microcrack lifetimes. Earth and Planetary Science Letters 113, 145–156.

Brantley, S.L., Evans, B., Hickman, S.H., Crerar, D.A., 1990. Healing of microcracks in quartz: implications for fluid flow. Geology 18, 136–139.

Bürgmann, R., Pollard, D.D., 1994. Strain accommodation about strike-slip discontinuities in granite rock under brittle-to-ductile conditions. Journal of Structural Geology 12, 1655–1674.

Charbonneau, G.-P., Delugeard, Y., 1977. Biphenyl: three-dimensional data and new refinement at 293 K. Acta Crystallographica B33, 1586–1588.

Chester, F.M., 1988. The brittle-ductile transition in a deformation mechanism map for halite. Tectonophysics 154, 125–136.

Cox, S.F., 1999. Deformational controls on the dynamics of fluid flow in mesothermal gold systems. In: McCaffrey, K., Lonergan, L., Wilkinson, J. (Eds.), Fractures, Fluid Flow and Mineralization. Geological Society Special Publication 155, pp. 123–139.

Cox, S.F., Knackstedt, M.A., 1999. Ore genesis in fracture controlled hydrothermal systems: percolation theory approaches. Proceedings International Congress on Earth Sciences, Exploration and Mining around the Pacific Rim — PACRIM'99, pp. 639–642.

Cox, S.F., Etheridge, M.A., Wall, V.J., 1987. The role of fluids in syntectonic mass transport, and localization of metamorphic vein-type ore deposits. Ore Geology Reviews 2, 65–86.

Etheridge, M.A., 1983. Differential stress magnitudes during regional deformation and metamorphism: Upper bound imposed by tensile fracturing. Geology 11, 231–234.

Etheridge, M.A., Wall, V.J., Vernon, R.H., 1983. The role of the fluid phase during regional metamorphism and deformation. Journal of Metamorphic Geology 1, 205–226.

Etheridge, M.A., Wall, V.J., Cox, S.F., Vernon, R.H., 1984. High fluid pressures during regional metamorphism and deformation: implications for mass transport and deformation mechanisms. Journal of Geophysical Research 89, 4344–4358.

Glazner, A.F., Bartley, J.M., 1991. Volume loss, fluid flow and state of strain in extensional mylonites from the central Mojave Desert, California. Journal of Structural Geology 13, 587–594.

Hacker, B.R., Christie, J.M., 1990. Brittle/ductile and plastic/cataclastic transitions in experimentally deformed and metamorphosed amphibolite. In: Duba, A.G., Durham, W.B., Handin, J.W., Wang, H.F. (Eds.), The Brittle-Ductile Transition in Rocks, The Heard Volume. Geophysical Monograph 56, pp. 127–147.

Handin, J., Hager Jr, R.V., Friedman, M., Feather, J.N., 1963. Experimental deformation of sedimentary rocks under confining pressure: pore pressure tests. Bulletin of the American Association of Petroleum Geologists 47, 718–755.

Handy, M.R., Streit, J.E., 1999. Mechanics and mechanisms of magmatic underplating: inferences from mafic veins in deep crustal mylonite. Earth and Planetary Science Letters 165, 271–286.

Henderson, I.H.C., McCaig, A.M., 1996. Fluid pressure and salinity variations in shear zone-related veins, central Pyrenees, France: Implications for fault-valve model. Tectonophysics 262, 321–348.

Herwegh, M., Handy, M.R., 1996. The evolution of high-temperature mylonitic fabrics: evidence from simple shearing of a quartz analog (norcamphor). Journal of Structural Geology 18, 689–710.

Herwegh, M., Handy, M.R., 1998. The origin of shape preferred orientations in mylonite: inferences from in-situ experiments on polycrystalline norcamphor. Journal of Structural Geology 20, 681–694.

Hickman, S., Sibson, R., Bruhn, R., 1995. Introduction to special session: mechanical involvement of fluids in faulting. Journal of Geophysical Research 100, 12,831–12,840.

Kerrich, R., 1986. Fluid infiltration into fault zones: chemical, isotopic, and mechanical effects. Pure and Applied Geophysics 124, 225–268.

Kerrich, R., Allison, I., 1978. Vein geometry and hydrostatics during Yellowknife mineralisation. Canadian Journal of Earth Sciences 15, 1653–1660.

Law, R.D., 1998. Oblique grain-shape fabrics in a mylonite quartz vein. In: Snoke, A.W., Tullis, J., Todd, V.R. (Eds.), Fault-related Rocks — A Photographic Atlas. Princeton University Press, Princeton, New Jersey, pp. 264–265.

Lister, G.S., Snoke, A.W., 1984. S–C Mylonites. Journal of Structural Geology 6, 617–638.

Logan, J.M., Dengo, C.A., Higgs, N.G., Wang, Z.Z., 1992. Fabrics of experimental fault zones: their development and relationship to mechanical behavior. In: Evans, B., Wong, T.-F. (Eds.), Fault Mechanics and Transport Properties of Rocks. Academic Press, London, pp. 33–67.

McCaig, A.M., 1988. Deep fluid circulation in fault zones. Geology 16, 867–870.

McCaig, A.M., Wickham, S.M., Taylor Jr, H.P., 1990. Deep fluid circulation in alpine shear zones, Pyrenees, France: field and oxygen isotope studies. Contributions to Mineralogy and Petrology 106, 41–60.

Means, W.D., 1989. Synkinematic microscopy of transparent polycrystals. Journal of Structural Geology 11, 163–174.

Murrell, S.A.F., 1965. The effect of triaxial stress systems on the strength of rocks at atmospheric temperatures. Journal of the Geophysical Royal Astronomical Society 10, 231–281.

Nguyen, P.T., Cox, S.F., Harris, L.B., Powell, C.McA., 1998. Fault-valve behaviour in optimally oriented shear zones: an example at the revenge gold mine, Kambalda, Western Australia. Journal of Structural Geology 20, 1625–1640.

O'Hara, K., 1988. Fluid flow and volume loss during mylonitization: an origin for phyllonite in an overthrust setting, North Carolina, USA. Tectonophysics 156, 21–36.

O'Hara, K., 1990. Brittle-plastic deformation in mylonites: an example from the Meadow Fork thrust, western Blue Ridge province, southern Appalachians. Geological Society of America Bulletin 102, 1706–1713.

Robert, F., Boullier, A.-M., Firdaous, K., 1995. Gold-quartz veins in metamorphic terranes and their bearing on the role of fluids in faulting. Journal of Geophysical Research 100, 12,861–12,879.

de Roo, J.A., Williams, P.F., 1990. Dynamic recrystallization and solution transfer in mylonitic rocks of the Tetagouche Group, northern New Brunswick, Canada. Geological Society of America Bulletin 102, 1544–1554.

de Roo, J.A., Weber, K., 1992. Laminated veins and hydrothermal breccia as markers of low-angle faulting, Rhenish Massif, Germany. Tectonophysics 208, 413–430.

Sahimi, M., 1994. Applications to Percolation Theory. Taylor & Francis, London.

Schmid, S.M., Handy, M.R., 1991. Towards a classification of fault rocks: geological usage and tectonophysical implications. In: Müller, D.W., McKenzie, J.A., Weissert, H. (Eds.), Controversies in Modern Geology: Evolution of Geological Theories in Sedimentology, Earth History and Tectonics. Academic Press, London, pp. 339–360.

Selverstone, J., Morteani, G., Staude, J.-M., 1991. Fluid channelling during ductile shearing: transformation of granodiorite into aluminous schist in the Tauern Window, Eastern Alps. Journal of Metamorphic Geology 9, 419–431.

Sibson, R.H., 1985. Stopping of earthquake ruptures at dilational fault jogs. Nature 316, 248–251.

Sibson, R.H., 1986. Earthquakes and rock deformation in crustal fault zones. Annual Reviews of Earth and Planetary Sciences 14, 149–175.

Simpson, C., 1998. Heterogeneous deformation of tonalite and pegmatite vein. In: Snoke, A.W., Tullis, J., Todd, V.R. (Eds.), Fault-related Rocks — A Photographic Atlas. Princeton University Press, Princeton, New Jersey, pp. 232–233.

Stel, H., 1981. Crystal growth in cataclasites: diagnostic microstructures and implications. Tectonophysics 78, 585–600.

Stel, H., Lankreyer, A.C., 1994. Flow and deformation of viscous, silica-oversaturated dispersions in low-grade faults. Journal of Structural Geology 16, 303–313.

Streit, J.E., 1997. Low frictional strength of upper crustal faults: A model. Journal of Geophysical Research 102, 24,619–24,626.

Streit, J.E., 1998. Multiple generation cataclasites. In: Snoke, A.W., Tullis, J., Todd, V.R. (Eds.), Fault-related Rocks — A Photographic Atlas. Princeton University Press, Princeton, New Jersey, pp. 54–55.

Streit, J.E., Cox, S.F., 1998. Fluid infiltration and volume change during mid-crustal mylonitization of Proterozoic granite, King Island, Tasmania. Journal of Metamorphic Geology 16, 179–212.

Streit, J.E., Cox, S.F., 2000. Asperity interactions during creep of simulated faults at hydrothermal conditions. Geology 28, 231–234.

Swanson, M.T., 1988. Pseudotachylyte-bearing strike-slip duplex structures in the Fort Foster Brittle Zone, S. Maine. Journal of Structural Geology 10, 813–828.

Takagi, H., 1998. Foliated fault gouges. In: Snoke, A.W., Tullis, J., Todd, V.R. (Eds.), Fault-related Rocks — A Photographic Atlas. Princeton University Press, Princeton, New Jersey, pp. 58–59.

Tchalenko, J.S., 1970. Similarities between shear zones of different magnitudes. Geological Society of America Bulletin 81, 1625–1640.

Tullis, J., Yund, R.A., 1980. Hydrolytic weakening of experimentally deformed Westerly granite and Hale albite rock. Journal of Structural Geology 2, 439–451.

Urai, J.L., 1987. Development of microstructure during deformation of carnallite and bischofite in transmitted light. Tectonophysics 135, 251–263.

Urai, J.L., Humphreys, F.J., Burrows, S.E., 1980. In-situ studies of the deformation and dynamic recrystallization of rhombohedral camphor. Journal of Materials Science 15, 1231–1240.

Zhang, S., Cox, S.F., Paterson, M.S., 1994. The influence of room temperature deformation on porosity and permeability in calcite aggregates. Journal of Geophysical Research 99, 15,761–15,775.